Northumbria Research Link

Citation: Teo, Tiong Teck, Logenthiran, Thillainathan, Woo, Wai Lok, Abidi, Khalid, John, Thomas, Wade, Neal S., Greenwood, David M., Patsios, Charalampos and Taylor, Philip C. (2021) Optimization of Fuzzy Energy-Management System for Grid-Connected Microgrid Using NSGA-II. IEEE Transactions on Cybernetics, 51 (1). pp. 5375-5386. ISSN 2168-2267

Published by: IEEE

URL: https://doi.org/10.1109/tcyb.2020.3031109 <https://doi.org/10.1109/tcyb.2020.3031109>

This version was downloaded from Northumbria Research Link: http://nrl.northumbria.ac.uk/id/eprint/45037/

Northumbria University has developed Northumbria Research Link (NRL) to enable users to access the University's research output. Copyright © and moral rights for items on NRL are retained by the individual author(s) and/or other copyright owners. Single copies of full items can be reproduced, displayed or performed, and given to third parties in any format or medium for personal research or study, educational, or not-for-profit purposes without prior permission or charge, provided the authors, title and full bibliographic details are given, as well as a hyperlink and/or URL to the original metadata page. The content must not be changed in any way. Full items must not be sold commercially in any format or medium without formal permission of the copyright holder. The full policy is available online: http://nrl.northumbria.ac.uk/policies.html

This document may differ from the final, published version of the research and has been made available online in accordance with publisher policies. To read and/or cite from the published version of the research, please visit the publisher's website (a subscription may be required.)

Northumbria University NEWCASTLE

University Library

Optimization of Fuzzy Energy Management System for Grid-Connected Microgrid Using NSGA-II

Tiong Teck Teo, *Member, IEEE,* Thillainathan Logenthiran, *Senior Member, IEEE,* Wai Lok Woo, *Senior Member, IEEE,* Khalid Abidi, *Member, IEEE,* Thomas John, *Member, IEEE,* Neal S. Wade, *Member, IEEE,* David M. Greenwood, *Member, IEEE,* Charalampos Patsios, and Philip C. Taylor, *Senior Member, IEEE*

***Abstract*—This paper proposes a fuzzy logic based energy management system (FEMS) for a grid-connected microgrid with renewable energy sources (RES) and energy storage system (ESS). The objectives of the FEMS are reducing the average peak load (APL) and operating cost through arbitrage operation of the ESS. These objectives are achieved by controlling the charge and discharge rate of the ESS based on the state-of-charge of ESS, the power difference between load and RES, and electricity market price. The effectiveness of the fuzzy logic greatly depends on the membership functions. The fuzzy membership functions of the FEMS are optimized offline using a Pareto based multi-objective evolutionary algorithm, nondominated sorting genetic algorithm (NSGA-II). The best compromise solution is selected as the final solution and implemented in the fuzzy logic controller. A comparison with other control strategies with similar objectives are carried out at a simulation level. The proposed FEMS is experimentally validated on a real microgrid in the energy storage test bed at Newcastle University, UK.**

***Index Terms*—energy storage management, membership function tuning, microgrid, multiobjective evolutionary algorithm.**

I. Introduction

Microgrids are small-scale power systems which contain renewable energy sources (RES) such as photovoltaic (PV) and wind power, demand, and control and energy management systems to allow them to operate independently from the main transmission and distribution system. The variability of the load and generation within a microgrid pose serious challenge to the stability and security of the power system [1]. Energy Storage Systems (ESS) are seen as a key enabling technology to mitigate these challenges. However, while capital costs have fallen significantly, large-scale ESS remain expensive. As such, the operation of a single ESS should provide multiple services to maximize its benefit [2].

ESS can provide services such as energy arbitrage and peak demand reduction. Energy arbitrage describes the process of charging the ESS when the cost of electricity is low and discharging when the cost is high. The ESS can thereby gain revenue by capitalizing on the price difference. Peak demand reduction is a technique to reduce the power consumption during the period(s) of maximum demand. The ESS charges when the demand is low and discharges when the demand is high; this can assist the power system operator to reduce or defer costly infrastructure expansion, avoid operating expensive peaking generators, and reduce network losses.

Several control strategies have been proposed for the energy management system (EMS) to enable the ESS to combine these services, including fuzzy logic-based EMS (FEMS) [3], fuzzy logic controller (FLC) for wind power smoothing [4], frequency response [5] and grid power smoothing [6]. These methods improve the operation of the ESS, the design process heavily rely on expert knowledge and optimization is not conventionally applied.

Mathematical optimization methods such as mixed-integer linear programming (MILP), stochastic programming and convex optimization can also be applied to the EMS. Day-ahead and week-ahead scheduling of ESS to maximize revenue is proposed in [7]. The bidding, scheduling and deployment of an ESS, solely for revenue maximization, using stochastic programming is proposed in [8]. A daily cost minimization using convex optimization by considering time-of-use tariffs and day-ahead forecast of solar PV is proposed in [9]. These methods aim to find the optimal solution for the respective objective function which can result in a large optimization problem. In order to achieve computational viability for real-time operation, they have to consider a smaller set of uncertainty scenarios or constraint relaxation For the EMS of a microgrid, many factors have to be considered besides revenue maximization, such as peak demand reduction [10], storage degradation [11], and real-time operation under uncertainty [12]–[14]. A multiobjective ESS in a grid-connected microgrid, with the objective of significantly reducing operating cost and power exchange is also investigated in [15].

An EMS based on Multi-Objective Optimization (MOO) is proposed in [16]–[18]. The operating cost and peak shaving of the microgrid are formulated as a single-objective optimization problem through scalarization [16]. The hydrogen consumption of the fuel cells and load variation are minimized to prolong the lifetime of the fuel cell using FLC in [17]. The parameters of the FLC are tuned using a genetic algorithm (GA). The economic cost and CO_2 equivalent emission are formulated as a day-ahead unit commitment problem and minimized using dynamic programming in [18]. These methods only produces a single solution and do not consider the trade-

T.T. Teo and K. Abidi are with the Electrical Power Engineering Program, Newcastle University in Singapore, Singapore.

T. Logenthiran is with the School of Engineering and Technology, University of Washington, Tacoma.

W.L. Woo is with the Department of Computer and Information Sciences, Northumbria University, United Kingdom.

Thomas John, Neal S. Wade, David M. Greenwood, Charalampos Patsios, and Philip C. Taylor are with the School of Engineering, Newcastle University, United Kingdom

The work in this paper was supported by the Engineering and Physical Sciences Research Council (EPSRC) under grant number EP/P001173/1 , and EP/N032888/1.

off between objective functions.

In MOO, no single solution exists to minimize both objectives simultaneously. However, there exists a set of Pareto optimal solutions. A solution is part of the Pareto set if none of the individual objective can be improved without deteriorating the other objective function. Without any additional information or preference, all Pareto optimal solutions are considered equally good [19].

Multi-objective evolutionary algorithm (MOEA) such as niched Pareto genetic algorithm (NPGA) [20], strength Pareto evolutionary algorithm (SPEA) [21] and non-dominant sorting algorithm II (NSGA-II) [22] can find a set of Pareto optimal solutions in a single run. It has been used in induction machine design [23], generation and transmission expansion planning [24], [25] and electric power optimal dispatch [26]–[28]. NSGA-II is able to find a more diverse solution on the Pareto-optimal front when compared to other multi-objective evolutionary algorithms [22], [29]–[31].

FLC based energy management system (FEMS) can be applied in real-time to manage variability of the load and RES. In FEMS, key parameters – including the membership functions (MF) and its fuzzy rules – are defined by expert knowledge. Determination of optimal FEMS parameters remains a challenge. Moreover, parameter optimization algorithms for FLC only focus on a single objective function [32].

The main contributions of this paper are:

1) A new method to simultaneously minimize the operating cost and peak demand of a microgrid by tuning the membership functions of a FEMS using NSGA-II;
2) an investigation into the trade-off between conflicting objective functions;
3) validating the real-time operational perforance of the proposed FEMS using the energy storage test bed in Newcastle University, UK.

The rest of this paper is organized as follows: the mathematical model of the microgrid and proposed FEMS are presented in section II; section III shows the implementation of NSGA-II to optimize the fuzzy membership functions; simulation studies and result can be found in section IV. The experimental validation of the proposed methodology is presented in Section V, and conclusions are drawn in Section VI.

II. Problem Formulations

This paper considers the problem of operating an ESS which is connected to a microgrid containing renewable generation sources. The problem is formulated using a fixed time step equal to the electricity market trading period. All system variables, constraints, and decisions are assumed constant for the duration of each time step. The rest of this section describes the mathematical models of the microgrid and ESS.

A. Grid-connected Microgrid Model

An overview of a grid-connected microgrid test system is shown in Fig. 1. This microgrid is similar to those considered in [3], [33], [34]; it contains RES (PV and wind generation), load, and an ESS. The RES and ESS are connected to a common DC bus via unidirectional and bidirectional DC/DC converters, respectively. The DC bus is coupled to the AC bus via a bidirectional DC/AC converter, and the AC bus is connected to the main grid and the AC load.

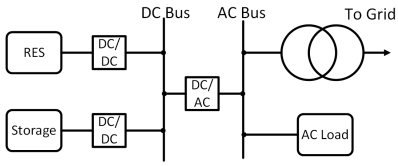

Fig. 1: Schematic of grid-connected microgrid

The power generated by the wind and PV generators are P_{wind} and P_{pv} respectively. Due to the intermittent nature of wind and PV, the power generated may be greater or less than the actual load, P_{load}. The difference between the actual load and renewable energy is expressed as $P_{balance}$. A positive $P_{balance}$ means the actual load is greater than the renewable power generated and a negative $P_{balance}$ means the renewable power generated exceeds the load as shown in (1).

$$P_{balance}(t) = P_{load}(t) - P_{wind}(t) - P_{pv}(t) \tag{1}$$

The ESS power set point, P_{ess}, varies to mitigate the imbalance as shown in (2). P_{grid} is the remaining power imbalance which must be met by the main grid.

$$P_{grid}(t) = P_{balance}(t) \pm P_{ess}(t) \tag{2}$$

B. Energy Storage System Model

Energy storage can be modeled by characterizing it in terms of power rating, energy capacity, and efficiency [35]. These characteristics are used to design the ESS model in this paper.

1) Power and Energy Limits: There are limits on the maximum power that can be imported or exported by an ESS; these limits can be expressed as follows.

$$0 \leq P_c(t) \leq \bar{P}_c \tag{3}$$

$$0 \leq P_d(t) \leq \bar{P}_d \tag{4}$$

where $\bar{P}_c$ and $\bar{P}_d$ are the maximum charging/discharging rate of the ESS. The maximum charging and discharging rate is considered in (3) and (4) in kW.

The energy limits of an ESS can be expressed using the state-of-charge (SoC).

$$SoC_{min} \leq SoC(t) \leq SoC_{max} \tag{5}$$

$$SoC_{model}(t) = SoC_{model}(t-1) + \frac{P_{ess}(t)\Delta t}{E_{max}} \tag{6}$$

where Δt is the assumed to be the duration of trading period of the electricity market, in a fifteen-minute basis and $SoC(t)$ expressed as a percentage.

2) Charging/Discharging Efficiency: When storing energy in an ESS, some energy will be lost in the conversions from AC to DC, from electricity to a storable form of energy, and when reversing these processes to supply power to the

network. These losses can be quantified by modelling the charging and discharging efficiencies of the system.

$$P_{ess}(t) = P_c(t) - P_d(t) \tag{7}$$

$$P_c(t) = \frac{p_c(t)}{\eta_c} \tag{8}$$

$$P_d(t) = p_d(t).\eta_d \tag{9}$$

where p, η and P are DC power, efficiency and AC power respectively. Subscripts c and d denotes charging and discharging. The power losses during conversion between DC/AC and AC/DC are considered in (8) and (9). The net output power of ESS is considered in (7) in kW.

C. Fuzzy Energy Management System

A Mamdani type FLC has been used as an EMS to control the charging and discharging rate of the ESS, an overview of which is shown in Fig. 2. It is a multi-input single-output FLC. The inputs are the power imbalance between the RES generation and consumers' demand, electricity market price, and ESS state-of-charge. These inputs are fed into the FLC to determine the charging and discharging rate of the ESS.

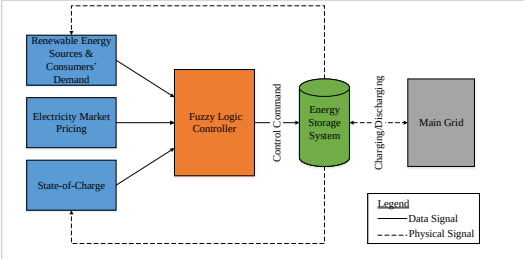

Fig. 2: Framework of the proposed fuzzy energy management system

The proposed fuzzy energy management system aims to:

1) Minimize the cost of energy bought and sold by the ESS
2) Reduce the average peak load (APL) of the microgrid
3) Avoid over and under charging of the ESS by maintaining the SoC within a upper and lower limits

The first and second aims are achieved by discharging the ESS during high demand or cost period and charge during low demand or cost period. The third aim is achieved by operating the ESS within the upper and lower limits. The proposed FLC is designed to reduce the consumers' electricity bill and reduce the power exchanged between the main and microgrid. The detailed design of this FEMS is discussed in [34].

III. Proposed NSGA-II for Tuning of Fuzzy Membership Functions

NSGA-II finds the Pareto-front quickly and efficiently compared to other multi-objective evolutionary algorithms such as Pareto-archived evolution strategy (PAES) and SPEA [22]. NSGA-II is used offline to optimize the locations of the membership function by minimizing the operating cost and APL of the microgrid while satisfying the constraints in Section II.

The GA starts with a population set which comprises randomly generated chromosomes, each representing fuzzy membership functions from the proposed FEMS. The chromosomes are evaluated using the fitness functions, domination count and crowding distance. After the chromosomes are evaluated, this population is evolved in through selection, crossover and mutation operators [36].

The selection operator chooses chromosomes with a higher fitness and assigns them to the set of parent chromosome, λ. This set then undergoes crossover and mutation to produce the chromosomes for the next generation.

In this paper, binary tournament selection is used to select the parents [37]. pairs of chromosomes are selected randomly and evaluates head-to-head; the fitter chromosome is then added to λ. This selection algorithm allows less-fit chromosomes to be selected because the fitness is relative to the opponent rather than the absolute fitness of the population. The fittest chromosome of the population is also added to λ to ensure elitism.

The crossover operator works on the principle that the fitter chromosomes comprising λ will combine to produce a better chromosome for the next generation. The chromosomes produced by the crossover operator is the offspring. A simulated binary crossover is used in this paper [38].

The mutation operator randomly selects chromosomes and alters them. This broadens the exploration of the search space and prevents the algorithm from becoming stuck in local minima.

The parent and offspring chromosomes from these operations are used in the next generation. This process is repeated until the termination condition is met. These processes are described in more detail in the following sections, and the full algorithm is summarized and in Algorithm 1.

A. Chromosome design

Each membership functions is coded as a string of real numbers, because precision is lost when the solutions are coded in binary, and moving to a neighboring solution requires changing many bits[39]. The type of encoding and the total number of membership functions determine the length of each chromosome.

Five membership functions are used to represent different linguistic terms for each input variable of the FLC. The membership functions tuned in this paper are triangular and trapezoidal. The membership functions are encoded into chromosomes, each of which represents a potential solution. Let chromosome be $C^g_{j,q}$.

$$C^g_{j,q} = \overbrace{x_1, \underbrace{x_2, x_3}_{m_2}, x_4}^{m_1}, ..., x_n \tag{10}$$

where q is the q^{th} chromosome within generation g for j^{th} variable, m_1 and m_2 are the first and second membership functions respectively. Fuzzy variable $P_{balance}$, ESS and P_{ess} comprises five triangular membership functions, each represented by a vector of three elements. From (11), the left span, center and right span of the triangle are a, b and c respectively.

$$f(x, a_n, b_n, c_n) = max\Big(min\Big(\frac{x - a_n}{b_n - a_n}, \frac{c_n - x}{c_n - b_n}\Big), 0\Big) \tag{11}$$

Algorithm 1: NSGA-II

1) **Chromosome Design**
2) **Initial Population** Generation, $G = G_k$
3) **while** *Termination Condition* $\neg$ **do**
   - **Fitness Function**
   - Evaluates the quality of each chromosome **for** *All chromosomes* **do**
     - **Nondominant Sorting**
     - Assign a domination count to each chromosome
     - **for** *Chromosomes with same domination count* **do**
       - **Calculate** Crowding distance
   - **Binary Tournament Selection**
   - From population P, select $\lambda = \{s_1, ..., s_\lambda\}$
   - $s = 1$
   - **for** $s \leq \lambda$ **do**
     - Randomly select two chromosome
     - Compare domination count and crowding distance
     - Put fitter chromsome into λ
     - $s = s + 1$
   - **Simulated Binary Crossover**
   - Select two parents x_1 and x_2
   - Compute offspring x_1^{new} and x_2^{new}
   - **Mutation**
   - Random select a chromosome from λ
   - Change a single gene in the chromosome
   - Sort the mutated chromosome in descending order.
   - **New population**
   - Combine parent and offspring population
   - $G = G_{k+1}$

Five triangular membership functions are used for $P_{balance}$, ESS and P_{ess} as shown in Fig. 3. From Table I, the center, b_1 and right span, c_1 of the first linguistic term, M_1 is equal to the left span, a_2 and center b_2 of the second linguistic term, M_2. This is to ensure that there is sufficient overlap between adjacent linguistic terms. Continuity is lost if the overlap is too small, and the linguistic term is redundant if overlap is too large. In this manner, five triangular membership functions can be represented using seven parameters, g_1 to g_7. The left, right and center of M_1 can be represented by g_1, g_2 and g_3 respectively.

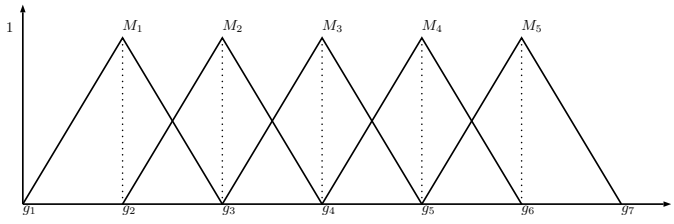

Fig. 3: $P_{balance}$ and ESS Membership Function

A randomly generated vector of 7 elements, g_1 to g_7, can represent the placement of all 5 triangular membership functions for $P_{balance}$ and ESS as shown in Table I.

TABLE I: Encoding $P_{balance}$ and ESS

$C_{j,q}^g$	x_1	x_2	x_3	x_4	x_5	x_6	x_7
M_1	a_1	b_1	c_1				
M_2		a_2	b_2	c_2			
M_3			a_3	b_3	c_3		
M_4				a_4	b_4	c_4	
M_5					a_5	b_5	c_5

The fuzzy membership function of C_p is similar to those of$P_{balance}$ and ESS, but contains trapezoids in addition to triangles. Fuzzy variable C_p contains 3 triangular membership functions and 2 trapezoid membership functions. The trapezoidal membership functions are represented by a vector of 4 elements. From (12), the left and right span are a and d. The "shoulders" are b and c.

$$f(x, a_n, b_n, c_n, d_n) = max\Big(min\Big(\frac{x - a_n}{b_n - a_n}, 1, \frac{d_n - x}{d_n - c_n}\Big), 0\Big) \tag{12}$$

Similar to the chromosome design of $P_{balance}$ and ESS, from Table II, the "right shoulder", c_1 and right span, d_1 of the first linguistic term M_1 is equal to the left span, a_2 and center, b_2 of the second linguistic term M_2. In this manner, two trapezoid and three triangle membership functions can be represented with nine parameters, g_1 to g_9.

Fig. 4 shows the membership functions for C_p.

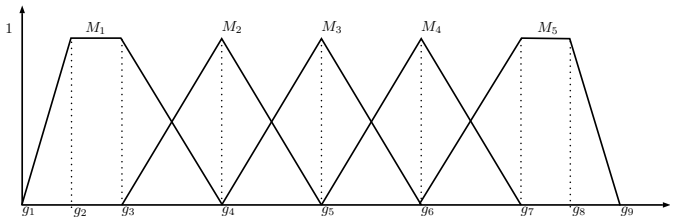

Fig. 4: C_p Membership Function

A randomly generated vector of 9 elements, g_1 to g_9 can represent the placement of all 5 membership functions for C_p, as shown in Table II.

TABLE II: Encoding C_p

$C_{j,q}^k$	x_1	x_2	x_3	x_4	x_5	x_6	x_7	x_8	x_9
M_1	a_1	b_1	c_1	d_1					
M_2			a_2	b_2	c_2				
M_3				a_3	b_3	c_3			
M_4					a_4	b_4	c_4		
M_5						a_5	b_5	c_5	d_5

B. Initial Population

The chromosomes are randomly generated and are subjected to the following constraints:

$$SoC_{min} \leq SoC(t) \leq SoC_{max} \tag{13}$$

$$P_{balance,min} \leq P_{balance}(t) \leq P_{balance,max} \tag{14}$$

$$C_{p,min} \leq C_p(t) \leq C_{p,max} \tag{15}$$

Constraint (13) restricts the upper and lower operating capacity of the ESS, which prevents over and under charging [40]. Constraints (14) and (15) are the maximum and minimum values of $P_{balance}$ and C_p, which are obtained from the historical data.

The maximum and minimum boundaries of these constraints can modified to suit any storage technology, electricity market price and microgrid configuration for which historical data are available.

C. Fitness Function

The fitness function evaluates the quality of each chromosome in a given generation. A poorly designed fitness function will result in a weak solution. The objective of the proposed FLC is to reduce the overall operating cost and APL by controlling the charging and discharging of the ESS. The overall operating cost of the microgrid can be calculated by (16).

$$f_1 = \sum_{t=1}^{T} P_{grid}(t).C_p(t) \tag{16}$$

where C_p is the wholesale electricity price. The microgrid can freely purchase and sell electricity from the main grid at time t at the same market price, $C_p(t)$.

a) $P_{grid}(t) > 0$ if electricity is purchased from the grid;
b) $P_{grid}(t) < 0$ if electricity is sold back to the grid.

The APL of the power profile is calculated using (17). The operating cost can be reduced by reducing the peak load of the power profile because the price is comparatively higher during this period.

$$f_2 = \frac{\sum_{m=1}^{\omega} P_{grid,max}(m)}{\omega} \tag{17}$$

where ω is the total number of months.

Because the objective of the FLC is to minimize operating cost and APL, equations (16) and (17) are used as fitness functions to evaluate each chromosome.

The focus of this paper is the operation of ESS, therefore the initial capital and maintenance cost of the ESS – which are considered during the system planning stages – are omitted from the operation cost. Furthermore, because the microgrid can be assumed small relative to the main grid, any arbitrage operation will have a negligible effect on the energy market price, therefore the microgrid is assumed to be a price taker.

A multi-objective optimization problem can be formulated as follows:

$$\begin{aligned} \min \quad & (f_1(x), f_2(x), ..., f_k(x)) \\ \text{s.t.} \quad & \forall x \in X \end{aligned} \tag{18}$$

where f, k, and x are the fitness function, k^{th} fitness function and x solution for the fitness function respectively. For instance, this paper considers (16) and (17) as the objective functions.

Let the fitness functions f_1, f_2 be (16) and (17). In addition to the fitness functions, domination count and crowding distance are computed to evaluate each solution.

1) Domination count and crowding distance: In multi-objective optimization, when considering the quality of two solutions, p and q, with multiple objective functions, i and j, solution p is considered to dominate solution q if:

1) $f_i(p) \leq f_i(q)$ for all indices $i \in 1, 2, ..., k$ and
2) $f_j(p) < f_j(q)$ for at least one index $j \in 1, 2, ...k$

When solution p is compared with q, if the fitness function for all objectives for p is less than or equal to q and p is less than q for at least one objective, p dominates q. If this criteria is not met, p and q are non-dominant and they belong to the same Pareto front (A set of non-dominated optimal solutions, in which no objective can be improved without deterioration of at least one other objective).

All solutions not dominated by any other solutions are assigned a domination count of 0. All solutions that are only dominated by solutions with domination count of 0 are assigned a domination count of 1. This process is repeated until all the solutions have a domination count. All solutions with the same domination count are considered equally good. The solutions with the same domination count are further differentiated by introducing a second entity, crowding distance.

Within the same Pareto front, the crowding distance is calculated. A higher crowding distance signifies a less crowded region, and vice-versa. When comparing two solutions with the same domination count, the solution with a higher crowding distance is the better solution. In this manner, the sorting algorithm favors a more diverse solution. The detailed implementation of domination count and crowding distance is found in [22].

2) Best Compromise Solution: Fuzzy set theory is implemented to determine the best compromise solution from the set of Pareto optimal solutions [26]. For each non-dominant solution k, the respective fitness function is fuzzified using (19).

$$\mu_i = \begin{cases} 1 & F_i \leq F_i^{min} \\ \frac{F_i^{max} - F_i}{F_i^{max} - F_i^{min}} & F_i^{min} < F_i < F_i^{max} \\ 0 & F_i \geq F_i^{max} \end{cases} \tag{19}$$

For each solution i, the maximum and minimum values are F_i^{max} and F_i^{min} respectively. The normalized membership function μ^k for each non-dominant solution, k, is calculated using (20).

$$\mu^k = \frac{\sum_{i=1}^{N_{obj}} \mu_i^k}{\sum_{j=1}^{M} \sum_{i=1}^{N_{obj}} \mu_i^j} \tag{20}$$

where M is the total number of non-dominant solutions and N_{obj} is the total number of objective functions. The solution with the highest value of μ^k is the best compromise solution. For each minimizing objective within the objective function, the lowest objective is assigned a value of 1 from (19).

D. Selection: Binary Tournament Selection

Binary tournament selection randomly chooses a pair of chromosomes from the population [37]. The domination count of the selected pairs are compared and the chromosome whose

domination count is lower is selected. If both chromosome have the same domination count, the chromosome with the higher crowding distance is selected. Elitism is ensured by selecting the solution with the highest crowding distance in the Pareto front and adding it to λ, the set of selected chromosomes.

E. Crossover & Mutation

Crossover produces the next generation of chromosomes based on the fittest chromosome from the current generation. The literature proposes several methods for crossover and mutation, which depend on how the chromosomes are encoded. Simulated Binary Crossover (SBX) simulates the single-point crossover operator of the binary-coded GAs. Let $C^g_{j,1}$ and $C^g_{j,2}$ be the two fittest chromosome of the g^{th} generation and j^{th} variable.

$$C^g_{j,1} = (c_1, ..., c_h, ..., c_z) \tag{21}$$

$$C^g_{j,2} = (c'_1, ..., c'_h, ..., c'_z) \tag{22}$$

where ϵ is a randomly generated number between 0 and 1, ψ is a distribution index which determines how similar the offspring is to the parent and β is the spread factor. The offspring solution of a large ψ are close to the parent solution and the offspring solution of a small ψ are far from the parent solution.

$$C^{g+1}_{j,1} = \frac{1}{2}[(1-\beta)C^g_{j,1} + (1+\beta)C^g_{j,2}] \tag{23}$$

$$C^{g+1}_{j,2} = \frac{1}{2}[(1+\beta)C^g_{j,1} + (1-\beta)C^g_{j,2}] \tag{24}$$

$$\beta = \begin{cases} (2\epsilon)^{\frac{1}{\psi+1}} & \text{if } \epsilon \leq 0.5 \\ (\frac{1}{2(1-\epsilon)})^{\frac{1}{\psi+1}} & \text{otherwise} \end{cases} \tag{25}$$

Random mutation is used in this paper to diversify the search space based using a predefined mutation probability, ρ_m.

IV. Simulation Results and Discussion

The proposed FEMS was implemented using MATLAB/Simulink. The parameters of the grid-connected microgrid used to test the FEMS are shown in Table III. The data used in this paper are obtained from the National Renewable Energy Laboratory (NREL) [41] and wholesale electricity prices from Energy Market Company Singapore (EMCSG). Time series data from January 1st 2013 to March 31st 2014, with a time step of 15 minutes, were used in this paper. The resulting dataset contained 43584 data points. The proposed FEMS aims to minimize the operating cost and APL from (16) and (17) of the grid-connected microgrid respectively by tuning the input fuzzy membership functions using NSGA-II.

TheNSGA-II algorithm described in Section II was implemented using a M-script file in MATLAB, and the FEMS was implemented in Simulink. The data from January 1st 2013 to December 31st 2013 were used to tune the FEMS and data from January 1st 2014 to March 31st 2014 were used to test the FEMS.

TABLE III: Microgrid Data

Parameter	Values
PV Array	13.68 kWp
Wind Turbine	12 kWp
Load	26.8 kWp
Energy storage capacity	90 kWh
Maximum charging\discharging rate	15kW
Upper and lower limit	90kWh, 4kWh
Charging\discharging efficiency, η_c, η_d	0.95

The chromosomes of the population were randomly generated according to Table III. The membership functions from each chromosome were encoded and evaluated in the FEMS. After all the chromosomes within the generation were evaluated, they were sorted using NSGA-II. These chromosomes then underwent crossover and mutation. This process was repeated until the maximum number of generations was met.

All of the parameters required by NSGA-II were determined heuristically, and are shown in Table IV.

TABLE IV: NSGA-II Parameters

	P	G	λ	ψ	ρ_c	ρ_m
Parameters	100	100	40	2	0.9	0.05

where P is the total number of chromosomes, G is the total number of generations, λ is the number of selected chromosomes for crossover, ψ is the crossover parameter, ρ_c and ρ_m are the crossover and mutation probability respectively.

Three case studies are presented in this paper as follows:

- Case study I: Minimizing operating cost
- Case study II: Minimizing APL
- Case study III: Multi-objective optimization

Case studies I and II were designed to find the extreme points of trade-off on the solution space with competing objective functions. Case studies I and II investigate single objective optimization, minimizing only cost or APL, respectively. In these cases, a standard GA was implemented. Case study III was a multi-objective optimization, in which cost and APL were minimized together. In this case, NSGA-II was implemented.

For each case study, the FEMS was tuned offline with historical data from 1 January 2013, to 31 December 2013, and validated online with data from 1 January 2014 to 31 March 2014. All case studies investigated the effect of adding the expert system fuzzy membership functions into the initial generation of GA/NSGA-II. As such, each case study is repeated twice. The first case, with expert system fuzzy membership functions as one of the chromosomes in the initial population, are labelled as $Predefined$ and the second, without any expert fuzzy membership functions, are labelled as $Random$.

As a comparison to NSGA-II for case study III, the two fitness functions, f_1 and f_2 from (16) and (17) were normalized using (26) and summed into a single figure of merit using (27). Normalizing both objective before summing them up gives an equal importance to both objectives instead of using weighted sum where additional weights parameter must be determined [42].

$$X' = \frac{X - min(X)}{max(X) - min(X)} \tag{26}$$

$$f_{agg} = f_1 + f_2 \tag{27}$$

The results of aggregated multi-objective optimization were compared with NSGA-II. Furthermore, an expert tuned FEMS was used as a comparison with the proposed methodology in each case study.

A. Case study I: Minimizing operating cost

This subsection presents the results and discussions for single objective optimization of operating cost using standard GA. The offline tuning and online validation results are shown in Table Va and Vb respectively. In offline tuning, the operating cost was reduced by approximately 5.5% and 3.8% in predefined and random. The APL reduced by 6.9% and 8.1% in predefined and random.

TABLE V: Minimizing operating cost

(a) Offline tuning of FEMS for minimizing operating cost

FEMS	Cost($)	APL(kW)	ΔPercentage (%)	
			Cost	APL
Expert FEMS	19246.5	12.5	-	-
GA Predefined	18188.1	11.6	-5.5	-6.9
GA Random	18507.9	11.5	-3.8	-8.1

(b) Online validation of FEMS for minimizing operating cost

FEMS	Cost($)	APL(kW)	ΔPercentage (%)	
			Cost	APL
Expert FEMS	4780.6	12.5	-	-
GA Predefined	4632.9	11.8	-3.1	-5.8
GA Random	4684.5	12.1	-2.0	-3.6

The GA with predefined membership functions in the initial population produced a better solution than random membership functions in terms of operating cost in this case study. Not only did it provide a lower operating cost, it also yielded a lower APL.

The reduction of population average fitness and fittest solution is shown in Fig. 5. GA with predefined expert knowledge membership functions can reach a lower operating cost faster than a random initialized GA.

B. Case study II: Minimizing APL

This subsection presents the results and discussions for single objective optimization of APL using a standard GA. From this subsection onward, the FEMS were tuned offline and only the online validation results are shown. The objective of case study II was to reduce the APL of the microgrid. The result of the online validation is shown in Table VI. The APL was reduced by approximately 21.2% and 11.4% for predefined and random respectively.

GA with predefined membership functions in the initial population produced a better solution than random membership functions in this case study. Not only did it provide a lower APL but also slightly reduced the operating cost.

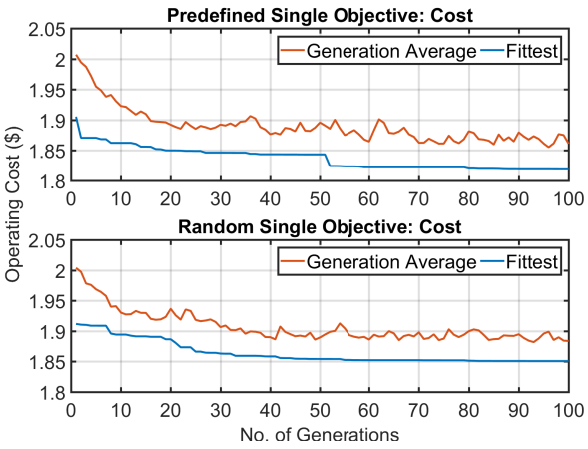

Fig. 5: Single Objective Optimization: Cost

TABLE VI: Online validation of FEMS for minimizing APL

FEMS	Cost($)	APL(kW)	ΔPercentage (%)	
			Cost	APL
Expert FEMS	4780.6	12.5	-	-
GA Predefined	4796.8	9.9	-0.3	-21.2
GA Random	4822.4	11.1	-0.9	-11.4

Similar to minimizing operating cost, GA with predefined expert membership functions can reach a lower APL faster than a random GA as shown in Fig. 6.

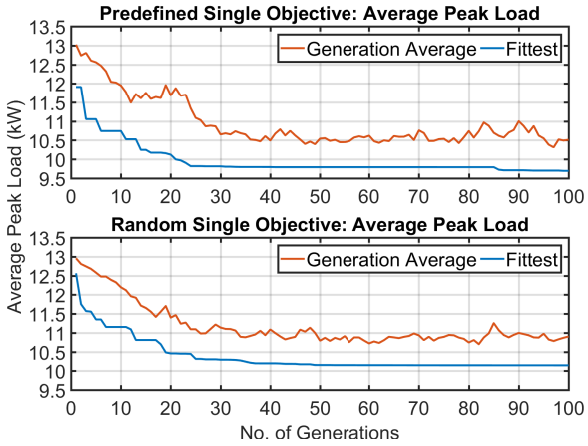

Fig. 6: Single Objective Optimization: Average Peak Load

In case studies I and II, having the expert tuned membership functions in the initial GA population yielded better results. For example in Case study I, even though minimizing operating cost was the objective function, both operating cost and APL were lower than the case where all initial chromosomes were random.

It is important to note that in online validation, for case study I: minimizing operating cost, the lowest operating cost was $4632.9 and with an APL of 11.8kW. In case study II: minimizing APL, the lowest APL was 9.9kW with an operating cost of $4796.8. These are the extreme points in the solution space, at the edges of the Pareto front. By comparing

the results in single objective optimization from Table Vb and VI, both objectives functions are in conflict. When the operating cost is minimized in case study I, the APL increases and vice-versa in case study II.

C. Case study III: Multi-objective optimization

Case study III compares three FEMS namely: an expert system from [34], aggregated multi-objective GA, and NSGA-II. Similar to case study I and II, aggregated multi-objective GA and NSGA-II were further separated into predefined and random. The online validation results are shown in Table VII.

The fittest solution from each generation is plotted onto the scatter heat maps shown in Fig. 7a and Fig. 7b illustrate the convergence of the GAs. Dark blue represents first generation, and dark red represents the 100^{th} generation. The optimum region is in the bottom left region of the heat map. From the first generation, the fittest solution of each generation improves and converges into the bottom left region through the genetic operators. In FEMS optimized using NSGA-II, by comparing Fig. 7c and Fig. 7d, the NSGA-II predefined have a more diverse Pareto front compared to NSGA-II random. NSGA-II predefined also have more solutions on the Pareto front.

As Table VII shows, the solutions obtained by different FEMS were fuzzified using (19) and (20) to obtain the μ^k. Among these solutions, NSGA-II predefined is the best compromise solution because it has the highest μ^k of 0.35. In the solution obtained by NSGA-II predefined, the operating cost and APL are decreased by 7.5% and 16.1% during offline tuning and 2.1% and 18.4% during online validation respectively.

TABLE VII: Best compromise solution for multi-objective optimization

FEMS	Cost ($)	APL (kW)	μ_1	μ_2	μ^k
Expert FEMS	4780.6	12.5	0.00	0.00	0.00
Aggregated predefined	4666.2	12.5	1.00	0.00	0.22
Aggregated random	4739.2	9.3	0.36	1.00	0.30
NSGA-II predefined	4681.9	10.2	0.86	0.72	0.35
NSGA-II random	4751.5	11.6	0.25	0.28	0.12

Fig. 8 shows the solutions for case studies I to III. From these case studies, the optimum solutions for case studies I and II are obtained from GA with predefined population. It is similar with case studies III as the best compromise solution is obtained with NSGA-II with predefined population. By comparing with the best solution from case study I and II, all three solutions belong to the same Pareto front as none of the solution dominates the other.

D. Simulated operation of FEMS using the best compromise solution

The best compromise solution from Section IV-C was used as the FEMS. Fig. 9 shows a one day of FEMS operation. From 0000 to 0600 hours, $P_{balance}$ was positive while the price was low. Hence the storage capitalized on this arbitrage opportunity to charge the storage. From 0800 to 1600 hours, $P_{balance}$ and C_p began to increase simultaneously; consequently, the storage discharged to reduce the peak demand. From 1600 to 2000 hours, the evening peak demand kicked in and the storage continued to discharge. From 2000 to 0000 hours, the SoC of the storage was approaching the minimum SoC, so the discharge rate gradually decreased to prevent over-discharging of the storage. The P_{grid} power profile fluctuated less compared to $P_{balance}$ as a result of FEM operation. The SoC of the storage also operated within the upper and lower boundary.

In multi-objective optimization, NSGA-II converges faster to the Pareto-optimal front when the initial population is initialized with expert membership functions. NSGA-II with predefined initial population has higher diversity. While NSGA-II can automatically generate all the membership functions for FEMS, empirical evidence from Case I and II have shown that the solution with predefined expert MF in the initial generation can yield a more diversified Pareto front and better solution.

Electricity was expensive during peak demand, so discharging during high price periods also reduced the peak demand [43]. Reducing peak demand can defer costly expansion of underutilized peaking power plant, transmission infrastructure, and distribution network. The APL was reduced by controlling the charging/discharging of the energy storage without altering the consumption of the consumer. The proposed methodology utilizes real-time electricity prices to enhance the operation of the ESS. It does not require the intervention of consumers to decide whether to buy or sell from the main grid. Furthermore, the proposed methodology utilizes the available resources without any changes or expansion to the current infrastructure of the microgrid. The proposed FEMS can be applied to other ESS operation as it is designed with historical data and parameters of the ESS.

V. Experimental Validation

The proposed methodology is experimentally validated in real-time using the energy storage test bed (ESTB) at Newcastle University, UK. An overview of the ESTB is shown in Fig. 10. The ESTB was connected to a 400V three phase network via a bi-directional AC/DC power converter rated at 360kVA, which then interfaces with the Northern Powergrid distribution network.

A. Energy storage test bed setup

1) 400V/400V Isolating Transformer: The ESTB is connected to the University network. The test bed is isolated from the main grid by this transformer.

2) Engineering station: The engineering station acts as a supervisory and control center for the ESTB. The proposed FEMS is implemented in MATLAB simulink model. The engineering station interfaces with the real-time target (RTT).

3) 700V DC busbar and power converters: The ESTB consisted of a single bi-directional AC/DC power converter rated at 360kVA and three bi-directional DC/DC power converters rated at 90kW each. These converters were connected to a common 700V DC bus. They were capable of setting different voltage, current and power set points either in real-time or from historical data.

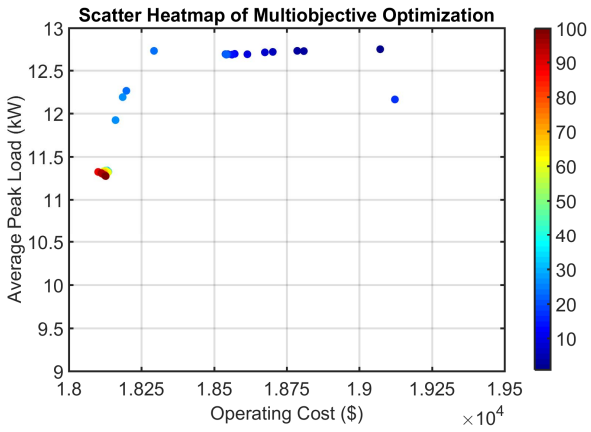

(a) Aggregated Predefined Multiobjective

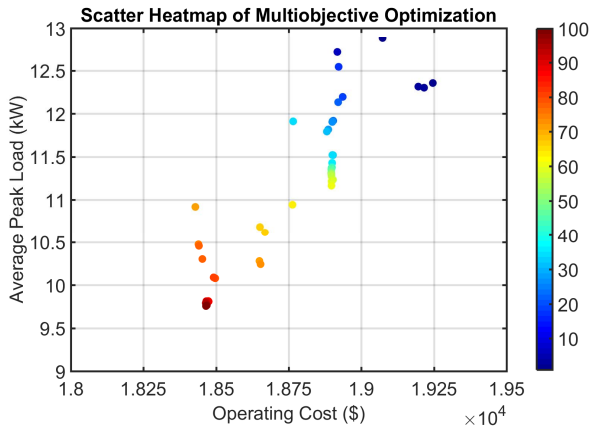

(b) Aggregated Random Multiobjective

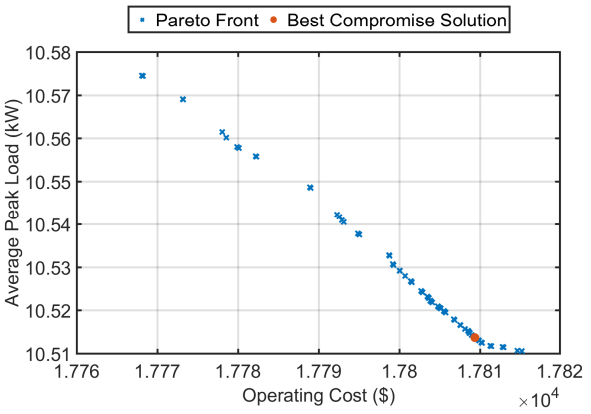

(c) NSGA-II Predefined Multiobjective

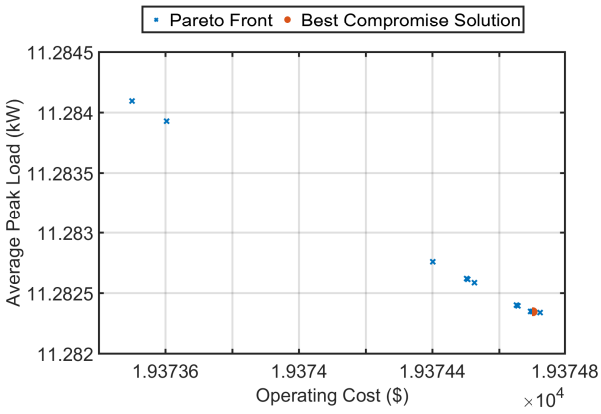

(d) NSGA-II Random Multiobjective

Fig. 7: Solution Space with Two Minimizing Objectives

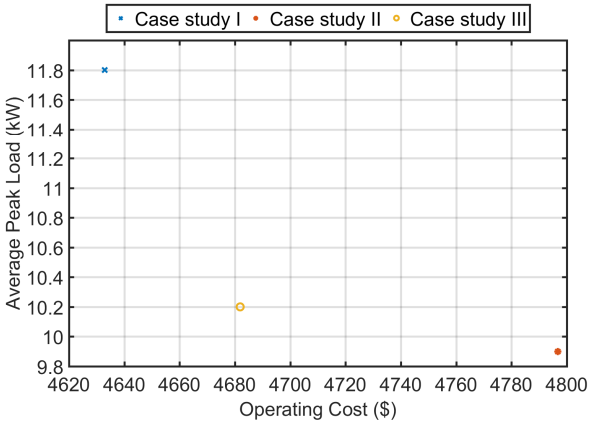

Fig. 8: Solutions of case studies I-III

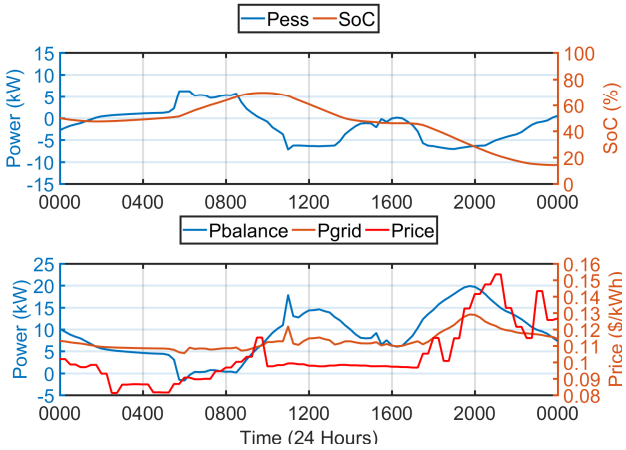

Fig. 9: Power profiles of simulation

4) Real-time target: The simulink model from the engineering station was compiled into a C program and executed in the RTT. The RTT controlled the voltage and current levels of the AC/DC converters, DC/DC converters and DC bus. This allowed real-time control of the power converters and ESS.

5) Energy storage system: A super-capacitor bank with ratings of 90 kW and 2 kWh was used in this experiment. The operating voltage was between 300V to 650V. This ESS was connected to the 700V DC bus via DC/DC converter.

This ESTB setup enabled experimental validation of the

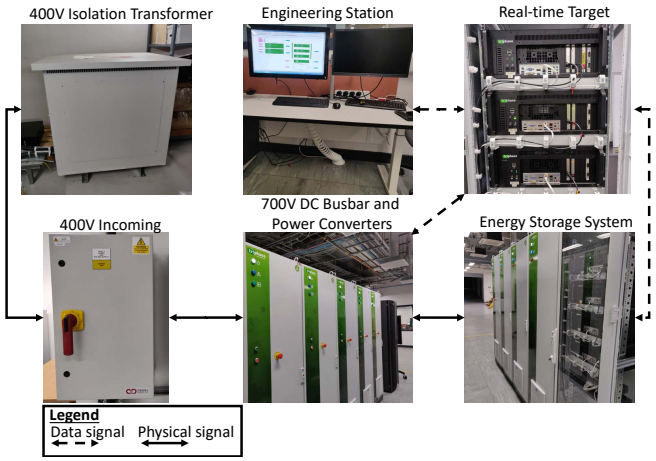

Fig. 10: Experimental setup of energy storage test bed

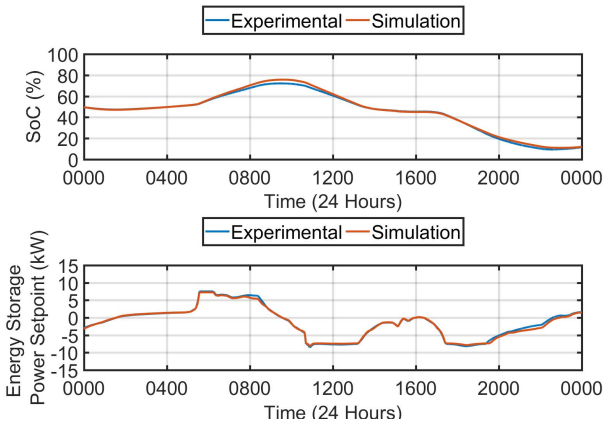

Fig. 11: Comparison between experimental and simulation results of the proposed FEMS

proposed control methodology in real-time and at grid-scale.

B. Experimental results

In the experiments presented, P_{load}, P_{pv}, and P_{wind} were represented using with data signals. This did not affect the results adversely, because the focus of this paper is the operation of ESS.

The time conversion from simulation to experimental is shown in Table VIII. Since the data signal is in 15 minutes interval (900s) and the ESTB runs in real-time, the ESTB operates 20 times faster. Where 1s in real-time corresponds to 45s in simulation time, as such 20s in real-time corresponds to 900s (15 minutes) in simulink. This allowed the 2kWh energy storage system to represent a 90 kWh system within the experiments.

TABLE VIII: Simulation to Experimental Time Conversion

	Time-step	Energy Capacity
Simulation	900s	90 kWh
Experiment	1s	2 kWh
Ratio	900:1	45:1

The SoC of the actual ESS was estimated using the open circuit voltage, V_{OC} and the operating voltage range, V_{max} and V_{min} as shown in (28) from [44], [45].

$$SoC_{actual} = \frac{V_{OC} - V_{min}}{V_{max} - V_{min}} \tag{28}$$

Fig. 11 compares the simulation power profile of ESS and SoC with the experiment. The SoC of the model can be accurately estimated using the generalized storage model from (6) and the actual ESS can follow the power setpoints from the proposed controller in real-time.

Mean absolute percentage error (MAPE) in (29) is used to quantify the agreement between the simulation model and experimental results. It is expressed as a percentage.

$$\text{MAPE} = \frac{100\%}{S} \sum_{t=1}^{S} \left| \frac{s(t) - e(t)}{s(t)} \right| \tag{29}$$

where S, s and e are the total number of samples, simulation data and experimental data for time t respectively.

From Table IX, the MAPE of SoC and Pess are 1.87% and 1.66% respectively. This shows excellent agreement between the model and experiment, thereby affirming the feasibility of the proposed approach in real systems.

TABLE IX: MAPE of simulation and experiment

	MAPE (%)
SoC	1.87
Pess	1.66

VI. Conclusion

This paper proposes a fuzzy based energy management system with three inputs and one output. The objectives are to minimize the operating cost and APL of the grid-connected microgrid with real-time pricing. The minimization of operating cost and APL is formulated into a multi-objective optimization problem with conflicting objective functions. Expert knowledge is integrated into the initial population of NSGA-II to obtain a diverse Pareto front in a single run. Three case studies were conducted in this paper. Case study I and II present a single objective optimization problem, where only operating cost or APL is minimized using standard GA. Case study III presents a multi-objective optimization problem by comparing an aggregated multi-objectives and NSGA-II. The results show that NSGA-II with expert knowledge in the initial population of GA is effective for handling multi-objective optimization with conflicting objective. NSGA-II is also able to obtain a diverse Pareto front. The proposed FEMS can be deployed to other power system with ESS with similar objectives as it is designed based on the historical data and not any specific storage technology. Furthermore, the proposed FEMS is experimentally validated and shows good agreement with the simulation.

References

[1] T. T. Teo, T. Logenthiran, and W. L. Woo, "Forecasting of photovoltaic power using extreme learning machine," in *2015 IEEE Innovative Smart Grid Technologies-Asia (ISGT ASIA)*. IEEE, 2015, pp. 1–6.

[2] R. H. Byrne, T. A. T. Nguyen, D. A. Copp, B. R. Chalamala, and I. Gyuk, "Energy management and optimization methods for grid energy storage systems," *IEEE Access*, vol. 6, pp. 13 231–13 260, 2018.

[3] T. T. Teo, W. L. Woo, T. Logenthiran, and K. Abidi, "Fuzzy logic control of energy storage system in microgrid operation," in *Innovative Smart Grid Technologies - Asia (ISGT-Asia), 2016 IEEE*. IEEE, 2016.

[4] F. Zhang, K. Meng, Z. Xu, Z. Dong, L. Zhang, C. Wan, and J. Liang, "Battery ess planning for wind smoothing via variable-interval reference modulation and self-adaptive soc control strategy," *IEEE Transactions on Sustainable Energy*, vol. 8, no. 2, pp. 695–707, April 2017.

[5] D. Greenwood, K. Lim, C. Patsios, P. Lyons, Y. Lim, and P. Taylor, "Frequency response services designed for energy storage," *Applied Energy*, vol. 203, pp. 115 – 127, 2017.

[6] D. Arcos-Aviles, J. Pascual, L. Marroyo, P. Sanchis, and F. Guinjoan, "Fuzzy logic-based energy management system design for residential grid-connected microgrids," *IEEE Transactions on Smart Grid*, vol. PP, no. 99, pp. 1–1, 2017.

[7] H. Khani and M. R. D. Zadeh, "Real-time optimal dispatch and economic viability of cryogenic energy storage exploiting arbitrage opportunities in an electricity market," *IEEE Transactions on Smart Grid*, vol. 6, no. 1, pp. 391–401, Jan 2015.

[8] H. Mohsenian-Rad, "Optimal bidding, scheduling, and deployment of battery systems in california day-ahead energy market," *IEEE Transactions on Power Systems*, vol. 31, no. 1, pp. 442–453, Jan 2016.

[9] Y. Wang, X. Lin, and M. Pedram, "A near-optimal model-based control algorithm for households equipped with residential photovoltaic power generation and energy storage systems," *IEEE Transactions on Sustainable Energy*, vol. 7, no. 1, pp. 77–86, Jan 2016.

[10] T. T. Teo, T. Logenthiran, W. L. Woo, and K. Abidi, "Near-optimal day-ahead scheduling of energy storage system in grid-connected microgrid," in *2018 IEEE Innovative Smart Grid Technologies - Asia (ISGT Asia)*, May 2018, pp. 1257–1261.

[11] C. Ju, P. Wang, L. Goel, and Y. Xu, "A two-layer energy management system for microgrids with hybrid energy storage considering degradation costs," *IEEE Transactions on Smart Grid*, vol. 9, no. 6, pp. 6047–6057, Nov 2018.

[12] Y. Neo, T. Teo, W. Woo, T. Logenthiran, and A. Sharma, "Forecasting of photovoltaic power using deep belief network," in *Region 10 Conference, TENCON 2017 - 2017 IEEE, At Penang, Malaysia, Malaysia*, 2017.

[13] V. De, T. T. Teo, W. L. Woo, and T. Logenthiran, "Photovoltaic power forecasting using lstm on limited dataset," in *2018 IEEE Innovative Smart Grid Technologies-Asia (ISGT Asia)*. IEEE, 2018, pp. 710–715.

[14] T. T. Teo, T. Logenthiran, and W. L. Woo, "Forecasting of photovoltaic power using regularized ensemble extreme learning machine," in *2016 IEEE Region 10 Conference (TENCON)*, 2016.

[15] T. T. Teo, T. Logenthiran, W. L. Woo, and K. Abidi, "Advanced control strategy for an energy storage system in a grid-connected microgrid with renewable energy generation," *IET Smart Grid*, vol. 1, no. 3, pp. 96–103, 2018.

[16] M. R. Sandgani and S. Sirouspour, "Energy management in a network of grid-connected microgrids/nanogrids using compromise programming," *IEEE Transactions on Smart Grid*, vol. PP, no. 99, pp. 1–1, 2017.

[17] R. Zhang and J. Tao, "Ga based fuzzy energy management system for fc/sc powered hev considering h2 consumption and load variation," *IEEE Transactions on Fuzzy Systems*, vol. PP, no. 99, pp. 1–1, 2017.

[18] H. Kanchev, F. Colas, V. Lazarov, and B. Francois, "Emission reduction and economical optimization of an urban microgrid operation including dispatched pv-based active generators," *IEEE Transactions on Sustainable Energy*, vol. 5, no. 4, pp. 1397–1405, Oct 2014.

[19] A. Zhou, B.-Y. Qu, H. Li, S.-Z. Zhao, P. N. Suganthan, and Q. Zhang, "Multiobjective evolutionary algorithms: A survey of the state of the art," *Swarm and Evolutionary Computation*, vol. 1, no. 1, pp. 32 – 49, 2011.

[20] J. Horn, N. Nafpliotis, and D. E. Goldberg, "A niched pareto genetic algorithm for multiobjective optimization," in *Proceedings of the First IEEE Conference on Evolutionary Computation. IEEE World Congress on Computational Intelligence*, Jun 1994, pp. 82–87 vol.1.

[21] E. Zitzler and L. Thiele, "An evolutionary algorithm for multiobjective optimization: The strength pareto approach," 1998.

[22] K. Deb, A. Pratap, S. Agarwal, and T. Meyarivan, "A fast and elitist multiobjective genetic algorithm: Nsga-ii," *IEEE Transactions on Evolutionary Computation*, vol. 6, no. 2, pp. 182–197, Apr 2002.

[23] L. A. Pereira, S. Haffner, G. Nicol, and T. F. Dias, "Multiobjective optimization of five-phase induction machines based on nsga-ii," *IEEE Transactions on Industrial Electronics*, vol. 64, no. 12, pp. 9844–9853, Dec 2017.

[24] P. Murugan, S. Kannan, and S. Baskar, "Application of nsga-ii algorithm to single-objective transmission constrained generation expansion planning," *IEEE Transactions on Power Systems*, vol. 24, no. 4, pp. 1790–1797, Nov 2009.

[25] M. R. AlRashidi and M. E. El-Hawary, "A survey of particle swarm optimization applications in electric power systems," *IEEE transactions on evolutionary computation*, vol. 13, no. 4, pp. 913–918, 2009.

[26] M. A. Abido, "Multiobjective evolutionary algorithms for electric power dispatch problem," *IEEE Transactions on Evolutionary Computation*, vol. 10, no. 3, pp. 315–329, June 2006.

[27] Y. Del Valle, G. K. Venayagamoorthy, S. Mohagheghi, J.-C. Hernandez, and R. G. Harley, "Particle swarm optimization: basic concepts, variants and applications in power systems," *IEEE Transactions on evolutionary computation*, vol. 12, no. 2, pp. 171–195, 2008.

[28] N. Sinha, R. Chakrabarti, and P. Chattopadhyay, "Evolutionary programming techniques for economic load dispatch," *IEEE Transactions on evolutionary computation*, vol. 7, no. 1, pp. 83–94, 2003.

[29] B. Ji, X. Yuan, and Y. Yuan, "Modified nsga-ii for solving continuous berth allocation problem: Using multiobjective constraint-handling strategy," *IEEE Transactions on Cybernetics*, vol. 47, no. 9, pp. 2885–2895, Sept 2017.

[30] E. Masazade, R. Rajagopalan, P. K. Varshney, C. K. Mohan, G. K. Sendur, and M. Keskinoz, "A multiobjective optimization approach to obtain decision thresholds for distributed detection in wireless sensor networks," *IEEE Transactions on Systems, Man, and Cybernetics, Part B (Cybernetics)*, vol. 40, no. 2, pp. 444–457, April 2010.

[31] K. Govindan, A. Jafarian, M. E. Azbari, and T. Choi, "Optimal bi-objective redundancy allocation for systems reliability and risk management," *IEEE Transactions on Cybernetics*, vol. 46, no. 8, pp. 1735–1748, Aug 2016.

[32] S. Wang, Y. Tang, J. Shi, K. Gong, Y. Liu, L. Ren, and J. Li, "Design and advanced control strategies of a hybrid energy storage system for the grid integration of wind power generations," *IET Renewable Power Generation*, vol. 9, no. 2, pp. 89–98, 2015.

[33] A. Merabet, K. T. Ahmed, H. Ibrahim, R. Beguenane, and A. M. Y. M. Ghias, "Energy management and control system for laboratory scale microgrid based wind-pv-battery," *IEEE Transactions on Sustainable Energy*, vol. 8, no. 1, pp. 145–154, Jan 2017.

[34] T. T. Teo, T. Logenthiran, W. L. Woo, and K. Abidi, "Intelligent controller for energy storage system in grid-connected microgrid," *IEEE Transactions on Systems, Man, and Cybernetics: Systems*, 2018.

[35] H. Ibrahim, A. Ilinca, and J. Perron, "Energy storage systems—characteristics and comparisons," *Renewable and Sustainable Energy Reviews*, vol. 12, no. 5, pp. 1221 – 1250, 2008.

[36] G. Syswerda, "Uniform crossover in genetic algorithms," in *Proceedings of the 3rd international conference on genetic algorithms*, 1989, pp. 2–9.

[37] B. L. Miller and D. E. Goldberg, "Genetic algorithms, tournament selection, and the effects of noise," *Complex systems*, vol. 9, no. 3, pp. 193–212, 1995.

[38] R. B. Agrawal, K. Deb, and R. Agrawal, "Simulated binary crossover for continuous search space," *Complex systems*, vol. 9, no. 2, pp. 115–148, 1995.

[39] K. Deep, K. P. Singh, M. L. Kansal, and C. Mohan, "A real coded genetic algorithm for solving integer and mixed integer optimization problems," *Applied Mathematics and Computation*, vol. 212, no. 2, pp. 505–518, 2009.

[40] I. Papic, "Simulation model for discharging a lead-acid battery energy storage system for load leveling," *IEEE transactions on energy conversion*, vol. 21, no. 2, pp. 608–615, 2006.

[41] C. Draxl, B. Hodge, A. Clifton, and J. McCaa, "Overview and meteorological validation of the wind integration national dataset toolkit," NREL/TP-5000-61740. Golden (CO): National Renewable Energy Laboratory (forthcoming), Tech. Rep., 2015.

[42] R. Wang, Z. Zhou, H. Ishibuchi, T. Liao, and T. Zhang, "Localized weighted sum method for many-objective optimization," *IEEE Transactions on Evolutionary Computation*, vol. PP, no. 99, pp. 1–1, 2016.

[43] J. C. Tee, T. Teo, T. Logenthiran, W. L. Woo, and K. Abidi, "Day-ahead forecasting of wholesale electricity pricing using extreme learning machine," in *Region 10 Conference, TENCON 2017 - 2017 IEEE, At Penang, Malaysia, Malaysia*, 2017.

[44] M. Ceraolo, G. Lutzemberger, and D. Poli, "State-of-charge evaluation of supercapacitors," *Journal of Energy Storage*, vol. 11, pp. 211 – 218, 2017.

[45] K. Mansiri, S. Sukchai, and C. Sirisamphanwong, "Fuzzy control algorithm for battery storage and demand side power management for economic operation of the smart grid system at naresuan university, thailand," *IEEE Access*, vol. 6, pp. 32 440–32 449, 2018.